

# Nanoscale

Accepted Manuscript



This is an *Accepted Manuscript*, which has been through the Royal Society of Chemistry peer review process and has been accepted for publication.

*Accepted Manuscripts* are published online shortly after acceptance, before technical editing, formatting and proof reading. Using this free service, authors can make their results available to the community, in citable form, before we publish the edited article. We will replace this *Accepted Manuscript* with the edited and formatted *Advance Article* as soon as it is available.

You can find more information about *Accepted Manuscripts* in the [Information for Authors](#).

Please note that technical editing may introduce minor changes to the text and/or graphics, which may alter content. The journal's standard [Terms & Conditions](#) and the [Ethical guidelines](#) still apply. In no event shall the Royal Society of Chemistry be held responsible for any errors or omissions in this *Accepted Manuscript* or any consequences arising from the use of any information it contains.

## ARTICLE

# Chemical Speciation of Heavy Metals by Surface-enhanced Raman Scattering Spectroscopy: Identification and Quantification of Inorganic- and Methyl-Mercury in Water

Cite this: DOI: 10.1039/x0xx00000x

Received 00th January 2012,  
Accepted 00th January 2012

DOI: 10.1039/x0xx00000x

www.rsc.org/

Luca Guerrini,<sup>a,b\*</sup> Ignacio Rodriguez-Loureiro,<sup>b,c</sup> Miguel A. Correa-Duarte,<sup>c</sup> Yih Hong Lee,<sup>d</sup> Xing Yi Ling,<sup>d</sup> F. Javier García de Abajo,<sup>e,f</sup> and Ramon A. Alvarez-Puebla.<sup>a,b,e\*</sup>

Chemical speciation of heavy metals has become extremely important in environmental and analytical research because of the strong dependence that toxicity, environmental mobility, persistence and bioavailability of these pollutants have on their specific chemical forms. Novel nano-optical-based detection strategies, capable of overcoming the intrinsic limitations of well-established analytic methods for the quantification of total metal ion content, have been reported, but the speciation of different chemical forms has not yet been achieved. Here, we report the first example of a SERS-based sensor for chemical speciation of toxic metal ions in water at trace levels. Specifically, the inorganic  $\text{Hg}^{2+}$  and the more toxicologically relevant methylmercury ( $\text{CH}_3\text{Hg}^+$ ) are selected as analytical targets. The sensing platform consists of a self-assembled monolayer of 4-mercaptopyridine (MPY) on highly SERS-active and robust hybrid plasmonic materials formed by a dense layer of interacting gold nanoparticles anchored onto polystyrene microbeads. Coordination of  $\text{Hg}^{2+}$  and  $\text{CH}_3\text{Hg}^+$  to the nitrogen atom of the MPY ring yields characteristic changes in the vibrational SERS spectra of the organic chemoreceptor that can be qualitatively and quantitatively correlated to the presence of the two different mercury forms.

## Introduction

Heavy metal ions are among the main pollutants of natural waters, representing a major concern to human health and the environment. Noteworthy, the toxicity of a specific metal ion does not only depend on its concentration level but is largely related to its chemical form. In fact, the speciation of a metal exercises a direct control over the environmental mobility, persistence and bioavailability.<sup>1,2</sup> Consequently, monitoring the distribution of the different chemical species, rather than the total metal content, is vital for a full understanding of their complex chemistry and their environmental and health effects. Highly sensitive analytical methods for metal cations detection and quantification commonly rely on atomic absorption or emission spectroscopy,<sup>3</sup> cold vapor atomic fluorescence spectrometry (CVAFS) and inductively coupled plasma-mass spectrometry (ICP-MS).<sup>4</sup> Speciation analysis requires, in addition, pre-separation procedures that are usually based on chromatographic methods or on different approaches that profit from the diverse chemical/physical properties of the metal species.<sup>4</sup> However, these traditional high-performance

techniques are generally expensive, time-consuming and incompatible with routine *in-situ* measurements. In this regard, there has been a growing interest in developing alternative detection strategies capable of overcoming the intrinsic limitations of these well-established analytic methods. The need for the development of fast, simple on-site monitoring techniques is even more acute in speciation analysis, as the sample collection, pre-treatments and storage are the most critical steps determining the sensitive and accurate quantification of often liable species. A paradigmatic case study is mercury and its compounds, which are listed among the most dangerous elements for human and ecosystem health.<sup>5,6</sup> In particular, methylmercury, produced in natural environments by anaerobic bacteria,<sup>7</sup> is the most potent mercuric toxins, the impact of which is severely worsened by its tendency to undergo extremely high bioaccumulation through the aquatic food web.<sup>4</sup> The high volatility of methylmercury and the dynamic interconversion processes between different species represent major obstacles in the exact determination of mercury species in natural waters.<sup>4</sup> Sensors based on electrochemical techniques,<sup>8</sup> and optical methods employing colorimetric,<sup>9-12</sup>

fluorometric,<sup>11, 13</sup> and surface-enhanced Raman scattering<sup>14-20</sup> outputs, are rapidly evolving into highly sensitive and robust devices capable of finally matching the stringent requirements for their translation to reliable applications in on-site real-life mercury analysis. However, one of the main challenges that still needs to be successfully tackled is the inability of these novel techniques to discriminate between different mercury species.<sup>1, 21</sup> In particular, all these reported strategies uniquely deal with the detection of the inorganic Hg<sup>2+</sup> form while the identification and quantification of the much more toxicologically relevant methylmercury is completely disregarded.

Surface-enhanced Raman scattering (SERS) spectroscopy is a vibrational spectroscopy that combines the intrinsically rich structural specificity and flexibility of Raman spectroscopy with the extremely high sensitivity provided by the dramatic intensification of the inelastic scattering from molecules located near/at nanostructured metal surfaces, where collective oscillations of conduction electrons of the plasmonic substrate are excited by interaction with light.<sup>22, 23</sup> As a result, SERS has arisen as a powerful analytical tool that has been implemented during the last decade in a myriad of different applications, particularly in the fields of environmental analysis and monitoring,<sup>24</sup> biodetection, diagnostics and bioimaging.<sup>25-27</sup> SERS has also been applied to the identification of vibrationless species, such as monoatomic metal ions, either via indirect methods that correlate changes in the absolute SERS intensity of a Raman label in the presence of the analyte<sup>14-17, 28</sup> or by direct detection when the atomic ions coordinate an organic chemoreceptor whose SERS spectrum contains characteristic spectral “fingerprints” that selectively informs about the type and extension of ion complexation.<sup>19, 29, 30</sup> The latter sensing approach offers several advantages<sup>31</sup> such as multiplexing capabilities.<sup>19, 29</sup>

Herein, we demonstrate the first example of the potential use of SERS for chemical speciation of heavy metal pollutants, specifically the identification and quantification at trace levels of Hg<sup>2+</sup> and CH<sub>3</sub>Hg<sup>+</sup> toxins in aqueous solution. The sensing strategy profits from the unique and characteristic spectral changes produced by the complexation of the inorganic and organic mercury forms with an organic ligand, which allow us to selectively identify and quantify at trace levels the presence of the two different species. As a metal ion receptor, we select 4-mercaptopyridine (MPY), which is known to strongly bind gold surfaces via its mercapto group and coordinate both mercuric species via the nitrogen of the pyridine moiety in water.<sup>32-35</sup> MPY is self-assembled onto closely spaced gold nanoparticles anchored on polystyrene microparticles, forming a hybrid plasmonic composite structure that acts as a robust and highly SERS-active platform supporting a dense collection of hot spots.<sup>30, 36</sup>

## Results and discussion

The fabrication of the Au NPs decorated polystyrene beads (PS@Au) was performed as previously described.<sup>30, 37</sup> Initially,

PS beads of 3 μm diameter were consecutively coated with layers of polyelectrolytes of opposite charge via a layer-by-layer assembly protocol. Specifically, negatively charged polystyrenesulfonate (PSS) and positively charged branched-polyethylenimine (PEI) were deposited in alternate fashion to yield a final external PEI shell with a compact collection of positive charges. Subsequently, a large excess of negatively charged citrate-coated gold nanoparticles of ~55 nm diameter were left to adhere by electrostatic interaction onto the so-functionalized PS beads, generating hybrid plasmonic microparticles with a dense homogenous coating of interacting nanostructures. Finally, extensive washing cycles were performed to ensure the removal of unbound nanoparticles. Figure 1A-B shows representative ESEM and TEM images of PS beads coated with Au nanoparticles (PS@Au), whereas Figure 1C-D illustrates the high resolution plasmonic characterization of an isolated PS@Au bead dried over a SiO<sub>x</sub>/Si substrate performed via cathodoluminescence (CL) hyperspectral imaging. Two maxima can be identified in the CL spectrum: a strong plasmon contribution at ~538 nm, attributed to longitudinal coupling of surface plasmon resonances between nanoparticles, and a weaker blue-shifted shoulder at ~504 nm, which we ascribe to dipolar plasmon modes of interacting nanoparticles and/or LSPR of isolated nanoparticles, both in vacuum.

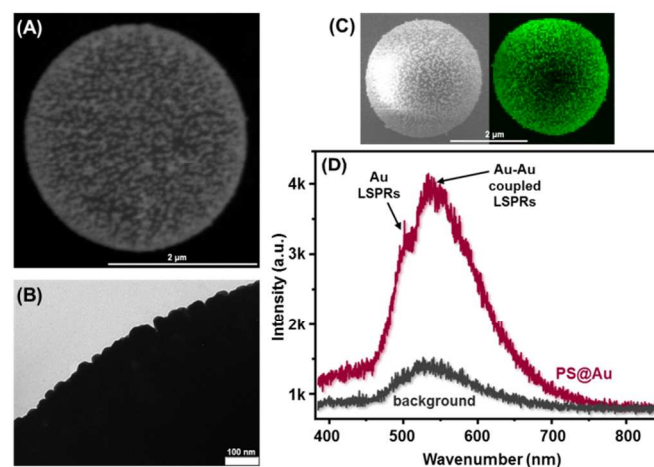


**Fig. 1** Representative ESEM (A) and TEM (B) images of PS@Au beads. (C) SEM image and photon map centered at 550 nm of a single PS@Au bead and (D) its corresponding CL spectrum.

These easily-fabricated composite materials behave as robust microscopic carriers of large ensembles of closely spaced nanoparticles, concentrating a high number of interparticle hot-spots in a dense external shell whose averaged plasmonic response ensures very good homogeneity from bead to bead SERS enhancing properties, as well as long-term optical stability.<sup>36, 38</sup> As a result, intense and reproducible SERS signals can be obtained with very low bead concentration in suspension, making such hybrid SERS substrates particularly suitable for sensing applications.<sup>30, 37</sup> Additionally, their resistance against aggregation offers a remarkable experimental flexibility regarding their manipulation and storage, which

largely lacks in their colloidal counterparts (for instance, centrifugation/redispersion steps can be performed at will without affecting the stability of the substrate, as well as changes in solvent, ionic strength etc.).

4-Mercaptopyridine (MPY) is a bifunctional molecule which is well-known to chemisorb onto Au surfaces via a metal-sulfur bond generating an ordered, densely packed monolayer where MPY molecules are preferentially oriented perpendicularly with respect to the metal surface, thus exposing the pyridinic nitrogen to the bulk solution.<sup>39, 40</sup> The corresponding SERS spectra of MPY have been thoroughly investigated and detailed vibrational band assignments can be found in the literature (the main band assignments and wavenumber positions are listed in Table S1).<sup>39, 41-44</sup> Figure 2 (green line) illustrates the characteristic MPY SERS spectrum at neutral pH.<sup>42</sup> It has been shown that coordination of metal ions to the pyridinic nitrogen atom leads to a redistribution of the electrons among different bonds within the aromatic ring, and such perturbation is directly reflected in the vibrational spectrum of the molecule.<sup>45-47</sup> This can be clearly observed in the MPY spectrum upon complexation with  $\text{Hg}^{2+}$  (Figure 2, blue curve), where remarkable alteration of the ligand spectral profile is revealed, in terms of both frequency shifts and relative intensities as further highlighted by digital subtraction of the SERS signal of the free ligand from the spectrum of the MPY- $\text{Hg}^{2+}$  surface complex (Figure 2, blue dotted curve). Several spectral features are worth commenting. First of all, we observe a general mild increase in frequency of the in-plane  $a_1$  pyridine modes such as those at  $702\text{ cm}^{-1}$ , ascribed to  $\beta(\text{CC})/\nu(\text{CS})$  modes, at  $1001\text{ cm}^{-1}$ , originating in pure ring breathing vibration, at  $1040\text{ cm}^{-1}$ , attributed to a  $\beta(\text{CH})$  mode, at  $1096\text{ cm}^{-1}$ , resulting from the mixed contributions of ring breathing and  $\nu(\text{CS})$  modes, and at  $1612\text{ cm}^{-1}$ , assigned to  $\nu(\text{C=C})/\nu(\text{C=N})$  vibrations. Secondly, we highlight a notable intensity increase of the mixed ring breathing/ $\nu(\text{CS})$  band at  $1096\text{ cm}^{-1}$ , and the band at  $1580\text{ cm}^{-1}$ , assigned to  $\nu(\text{C=C})/\nu(\text{C=N})$  vibrations that are characteristic of the N-deprotonated form, especially with respect to the features at  $1001$ ,  $1040$ ,  $1276$  and  $1612\text{ cm}^{-1}$ . Overall, such changes are consistent with the complexation of metal ions with the N atom of MPY.<sup>45-47</sup> Additionally, since attractive  $\pi$ - $\pi$  interactions between MPY molecules adsorbed on Au surfaces take place for high surface coverage,<sup>40</sup> we cannot rule out a cascade amplification where coordination of a metal ion on one pyridinic ring is indirectly “felt” by other proximal MPY molecules. It is worthy to note that the largest relative intensity decrease is recorded for the out-of-plane C-H deformation band at  $777\text{ cm}^{-1}$ . As we can reasonably expect that changes in the electron density of the aromatic ring only produce a poor perturbation of the modes involving hydrogen motions, this spectral change suggests a reorientation of the  $\text{Hg}^{2+}$ -coordinated-MPY molecules toward a more perpendicular position onto the metal surface, in agreement with the surface selection rules.<sup>48, 49</sup> Structural studies of pyridine (py) coordinated to  $\text{Hg}^{2+}$  in aqueous solution showed that  $\text{Hg}(\text{py})_n$

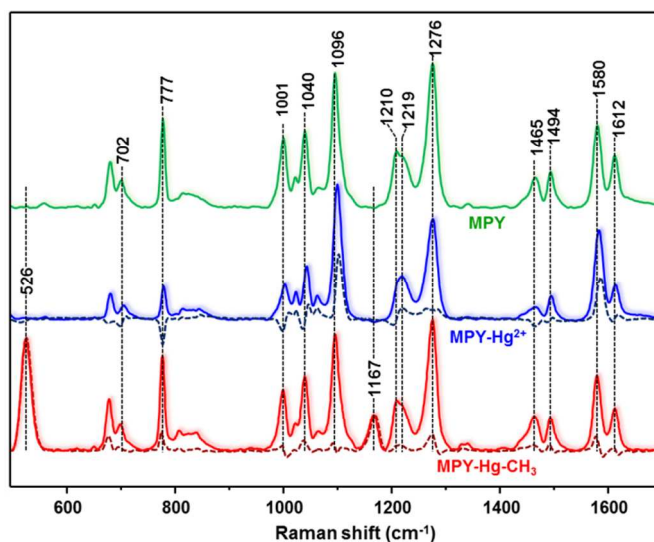


**Fig. 2** SERS spectra of 4-mercaptopyridine (MPY) on PS@Au beads before and after the exposure to  $\text{HgCl}_2$  20 ppb and  $\text{CH}_3\text{HgCl}$  15.1 ppb solutions (final concentration of beads in the analyte solution =  $0.8\text{ }\mu\text{g/mL}$ ). SERS spectra are normalized to the ring breathing band at  $1096\text{ cm}^{-1}$ . The dotted-curves are difference spectra obtained by subtracting the SERS of free MPY from the corresponding spectra in the presence of  $\text{HgCl}_2$  20 ppb and  $\text{CH}_3\text{HgCl}$  15.1 ppb. The Raman background of the plastic container (Figure S7) was subtracted from each spectrum (residual weak narrow bands at ca.  $808$  and  $841\text{ cm}^{-1}$ , ascribed to the plastic, may still appear in some spectra).

complexes predominantly exist for  $n = 2$  (and, to a lesser extent, for 3 and 4 pyridine unity),<sup>46</sup> and the metal coordination mostly occurs via  $\sigma$ -electron donation from the N to  $\text{Hg}^{2+}$  with negligible  $\pi$ -back bonding from the metal ion.<sup>32-34</sup> Thus, we can argue that chelation of  $\text{Hg}^{2+}$  via multidentate N-bonding is also favored with MPY molecules in the densely packed self-assembled monolayer that exists onto the gold surface.

In contrast, methylmercury ( $\text{CH}_3\text{Hg}^+$ ) has a strong tendency toward a linear two-coordinate geometry,<sup>34, 50, 51</sup> and therefore establish unidentate complexes with pyridine in solution with formation constants only slightly smaller than  $\text{Hg}(\text{py})_n$  ( $\text{pK}_a = 4.8$  for mono pyridine coordination with  $\text{CH}_3\text{Hg}^+$ <sup>55</sup> whereas the first two pyridine constants in  $\text{Hg}(\text{py})_2$  are almost equal: 5.1 and 4.9, respectively<sup>52</sup>). However, competing reactions in aqueous media generally reduce the extent to which  $\text{CH}_3\text{Hg}^+$  complexes organic ligands.<sup>35</sup> Figure 2 (red line) shows the SERS spectra of the MPY ligand in the presence of  $\text{CH}_3\text{Hg}^+$ . Strikingly, two new intense bands arise at  $526$  and  $1167\text{ cm}^{-1}$ , which are assigned to the stretching and bending modes, respectively, of the Hg-CH<sub>3</sub> group binding the MPY ligand.<sup>50, 53</sup> Importantly, when  $\text{CH}_3\text{Hg}^+$  directly adsorbed onto the unfunctionalized gold surface (Figure S4), the corresponding vibrational modes appear a very different wavenumbers, providing clear evidence of both the effective formation of the MPY- $\text{HgCH}_3$  complex and the existence of a densely packed self-assembled monolayer of the molecular receptor onto the metal nanoparticles that hampers the diffusion of the analyte to the gold surface. This conclusion is further supported by the lack of significant changes in the overall SERS intensity upon addition

of both mercury species (i.e. none/few MPY molecules were displaced from the metal surface by the analytes, see Figure S5A). Additionally, thiophenol (TP) was selected as a control molecule to investigate the potential intercalation of the mercury species in –S–Au bond. No changes in the SERS profile of TP were revealed even in the presence of high  $\text{Hg}^{2+}$  and  $\text{CH}_3\text{Hg}^+$  concentrations (i.e., no intercalation occurs, see Figure S5B), providing a further evidence that mercury-MPY interaction takes place via the aromatic nitrogen atom.

Unlike what was observed for  $\text{Hg}^{2+}$ , the SERS features of MPY are much less affected by the metal complexation with  $\text{CH}_3\text{Hg}^+$  (Figure 2, red dotted-line, difference spectrum obtained by removing the SERS signal of the free ligand from the spectrum of the MPY- $\text{HgCH}_3$  surface complex). This discrepancy from what we previously observed for  $\text{Hg}^{2+}$  coordination can be ascribed to the much weaker acid properties of  $\text{CH}_3\text{Hg}^+$ , which is expected to produce a corresponding lower alteration of the electron density in the aromatic ring. Additionally, it is reasonable to speculate that the unidentate interaction of the  $\text{CH}_3\text{Hg}^+$  can perturb the orientation of the coordinated MPY molecules much less than the adoption of a multidentate geometry around the  $\text{Hg}^{2+}$  ion.

The SERS response of the sensing device was also tested against several other ions, such as  $\text{Mg}^{2+}$ ,  $\text{Pb}^{2+}$ ,  $\text{Ni}^{2+}$ ,  $\text{Co}^{2+}$ ,  $\text{Cd}^{2+}$  and  $\text{Zn}^{2+}$ . The SERS spectrum of the ligand was left completely or largely unaltered upon addition of such metals at high concentration ( $10^{-6}$  M, Figure S6), thus indicating that MPY has excellent SERS selectivity for  $\text{Hg}^{2+}$  and  $\text{CH}_3\text{Hg}^+$ -sensing.

The differences in the spectral profiles of MPY coordinated either with inorganic or methylmercury are so remarkable that an effective SERS speciation can be easily achieved even without the need for any advanced multivariate data analysis. In fact, metal ion concentrations were quantitatively correlated with the spectral changes using the following ratiometric peak intensities: (a)  $I_{777}/I_{1096}$  for  $\text{Hg}^{2+}$  (ratio between the C-H deformation at  $777\text{ cm}^{-1}$  and the mixed ring breathing/ $\nu(\text{CS})$  band at  $1096\text{ cm}^{-1}$ , which showed the highest  $\pm$  variation rate in the presence of the analyte) and (b)  $I_{526}/I_{1096}$  for  $\text{CH}_3\text{Hg}^+$  (ratio between the most intense Hg- $\text{CH}_3$  vibrational feature in the spectrum and the ring breathing band at  $1096\text{ cm}^{-1}$ ).

Figure 3 illustrates four representative SERS spectra obtained in the presence of increasing  $\text{Hg}^{2+}$  amounts together with an inset figure describing the metal-ion-concentration-dependence of the  $I_{777}/I_{1096}$  ratio. SERS spectra were normalized to the band at  $1096\text{ cm}^{-1}$ , whereas the band at  $777\text{ cm}^{-1}$  was highlighted in blue to show its gradual weakening for increasing  $\text{Hg}^{2+}$  concentration. In the inset figure, three calibration lines are plotted, corresponding to data sets obtained at different PS@Au bead dilutions. The dynamic range for metal ion detection by SERS was indeed controlled by adjusting the beads concentration because, for our sensing purpose, a densely packed SAM of the molecular receptor is required onto the metal surface (i.e., the density of MPY binding sites onto the gold surface remain unchanged). The SERS spectra were then recorded by fixing the amount of

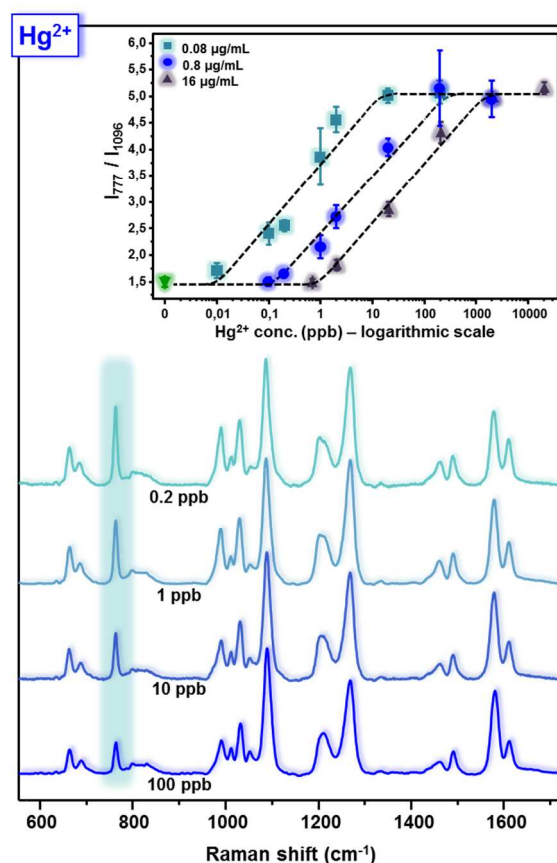


**Fig. 3** SERS spectra of MPY on PS@Au beads upon exposure to  $\text{HgCl}_2$  solutions of different concentration (final concentration of beads in solution =  $0.8\text{ }\mu\text{g/mL}$ ). SERS spectra are normalized to the ring breathing band at  $1096\text{ cm}^{-1}$ . Inset: intensity ratio,  $I_{1096}/I_{799}$ , of the MPY analyte-sensitive bands at  $1096$  and  $799\text{ cm}^{-1}$  as a function of  $\text{Hg}^{2+}$  concentration (logarithmic scale) for different bead concentrations in the metal ion solutions: (a)  $16\text{ }\mu\text{g/mL}$ , (b)  $0.8\text{ }\mu\text{g/mL}$  and (c)  $0.08\text{ }\mu\text{g/mL}$ . The corresponding detection limits are  $2\text{ ppb}$ ,  $0.1\text{ ppb}$  and  $50\text{ ppt}$ , respectively. Error bars are equal to two standard deviations ( $N = 3$ ).

PS@Au-MPY beads ( $10\text{ }\mu\text{L}$  of a  $0.4\text{ mg/mL}$  suspension) and exposing it to progressively larger volume of  $\text{Hg}^{2+}$  aqueous solutions ( $500\text{ }\mu\text{L}$ ,  $10\text{ mL}$  and  $50\text{ mL}$ , corresponding to  $16$ ,  $0.8$  and  $0.08\text{ }\mu\text{g/mL}$  final bead concentration, respectively). The mixtures were left under gentle shaking for 2 hours before being centrifuged to  $50\text{ }\mu\text{L}$  final volume, thoroughly sonicated and finally investigated by SERS in suspension. Pre-concentration of the beads to such small volume allows obtaining very intense SERS signals for short exposure time ( $10\text{ s}$ , 1 accumulation) with high spectral reproducibility, since the acquired SERS spectra are ensemble-average measurements of a large number

of PS@Au-MPY units. As can be seen from the inset in Figure 3, all plots of  $I_{777}/I_{1096}$  vs.  $\text{Hg}^{2+}$  concentration (ppb) reveal linear correlations for an interval of approximately 3 orders of magnitude (logarithmic scale), with progressively lower detection limits as the bead dilution is increased ( $2\text{ ppb}$ ,  $0.1\text{ ppb}$  and  $50\text{ ppt}$ , respectively) and high-quality squared correlation coefficient values ( $r^2 = 0.98$ ,  $0.99$  and  $0.94$ , respectively).

Importantly, the sensitivity of the sensor response (i.e. the slope of the regression line) remains constant regardless the bead dilution. Thus, a detection limit of several orders of magnitude lower than the U.S.A. EPA-defined maximum level of drinking water<sup>54</sup> has been easily achieved by trivial sample dilution thanks to the high SERS activity and optical stability of the PS@Au beads. We foresee, for instance, that the simple incorporation of PS@Au beads in common microfluidic channels for analyte accumulation would further increase the sensitivity of this method.

In qualitative agreement with the observation of Figure 2, the quantitative spectral response of MPY upon exposure to  $\text{CH}_3\text{Hg}^+$  solution at increasing concentrations diverges from the  $\text{Hg}^{2+}$  behavior. SERS spectra and plot (A) in Figure 4 indicate a linear increase of the  $I_{526}/I_{1096}$  ratio in the ~0-15 ppb range of analyte concentration for a final bead concentration of 0.8  $\mu\text{g}/\text{mL}$  (linear scale;  $r^2 > 0.98$ ; limit of detection 1.5 ppb). Once again, the SERS spectra were normalized to the band at 1096  $\text{cm}^{-1}$ , whereas the  $\nu(\text{Hg}-\text{CH}_3)$  band at 526  $\text{cm}^{-1}$  was highlighted in yellow. The high limit of detection achieved for  $\text{CH}_3\text{Hg}^+$  as compared to  $\text{Hg}^{2+}$  under the same experimental conditions (1.5 ppb vs. 0.1 ppb, respectively, for final concentration of beads in solution = 0.8  $\mu\text{g}/\text{mL}$ ) is consistent with the lower affinity of this soft Lewis acid for pyridinic ligands. Interestingly, in this case a saturation plateau of the  $I_{526}/I_{1096}$  ratio is not reached for higher  $\text{CH}_3\text{Hg}^+$  concentration but, on the contrary, a notable drop in the relative intensity of the  $\nu(\text{Hg}-\text{CH}_3)$  band is observed. As a representative example, the SERS spectrum obtained in the presence of  $\text{CH}_3\text{Hg}^+$  216 ppb is illustrated in Figure 4, pink curve. Here we observe, as for  $\text{Hg}^{2+}$ , a marked relative intensity increase of the ring breathing/ $\nu(\text{CS})$  band at 1096 and the “N-deprotonated” feature at 1580  $\text{cm}^{-1}$ , especially compared to the pure ring breathing contribution at 1001  $\text{cm}^{-1}$  and that of the “N-protonated” band at 1612  $\text{cm}^{-1}$ . Such features also undergo a slight red-shift of their peak position. However, differently to what occurred for  $\text{Hg}^{2+}$ , the out-of-plane C-H deformation band at 777  $\text{cm}^{-1}$  and the in plane C-H bending at 1040  $\text{cm}^{-1}$  do not suffer from relevant alterations of both their relative intensity and peak position. This peculiar change in spectral pattern is independent of the  $\text{CH}_3\text{Hg}^+$  concentration in the bulk and occurs at approximately the same [analyte]/[beads] ratio (Figure S8 and S9), indicating that the transition from these two different coordination regimes is mainly related to the analyte surface crowding. These findings seem to suggest a chemical transformation of the pyridine-coordinated  $\text{CH}_3\text{Hg}^+$  species when a threshold surface density is achieved. Nonetheless, as highlighted in Figure 4, plot B, the  $I_{777}/I_{1096}$  ratio in the detection of  $\text{CH}_3\text{Hg}^+$  shows minimal variation around the free ligand sample value even for high analyte concentration, thus preserving the spectral differentiation between the two mercury species.

Interestingly, SERS analysis of premixed inorganic/organic mercury solutions at ppb levels reveal spectral changes in the MPY vibrational profile that are solely ascribed to the coordination of  $\text{Hg}^{2+}$  (Figure 5A, blue curve, for  $\text{Hg}^{2+}$  and  $\text{CH}_3\text{Hg}^+$ , 3 ppb and 12 ppb, respectively). In contrast, when the

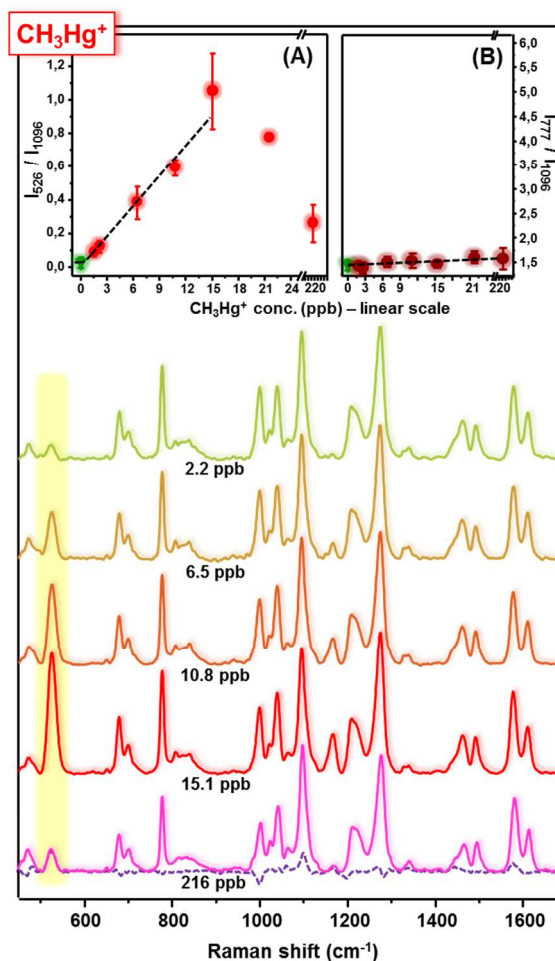


**Fig. 4** SERS spectra of MPY on PS@Au beads upon the exposure to  $\text{CH}_3\text{Hg}^+$  solutions of different concentrations (final concentration of beads in solution = 0.8  $\mu\text{g}/\text{mL}$ ). SERS spectra are normalized to the ring breathing band at 1096  $\text{cm}^{-1}$ . Insets: (A) intensity ratio,  $I_{526}/I_{1096}$ , of the  $\nu(\text{Hg}-\text{CH}_3)$  band at 526  $\text{cm}^{-1}$  and the MPY ring breathing band at 1096  $\text{cm}^{-1}$  (detection limit 1.5 ppb) and (B) intensity ratio,  $I_{777}/I_{1096}$ , of the MPY bands at 1096 and 799  $\text{cm}^{-1}$ , as a function of  $\text{CH}_3\text{Hg}^+$  concentration (linear scale; bead concentration in the metal solutions equals to 0.8  $\mu\text{g}/\text{mL}$ ). Error bars are equal to two standard deviations ( $N = 3$ ).

addition of  $\text{Hg}^{2+}$  is performed in a second step after the coordination of  $\text{CH}_3\text{Hg}^+$  to MPY, the characteristic methylmercury features, such as the intense band at 526  $\text{cm}^{-1}$  (Figure 5A, red curve) are retained in the SERS spectrum of the mixture (Figure 5A, green curve). These results suggest that, under the investigated experimental conditions, an extended decomposition of the methylmercury form is triggered in solution by the presence of the inorganic  $\text{Hg}^{2+}$ , unless  $\text{CH}_3\text{Hg}^+$  species are previously stabilized by coordination to MPY ligand (Figure 5B and C tentatively outline the two different processes). These findings are consistent with the dynamic interconversion of the two species in water, specifically with the shift of the equilibrium from the chemically labile  $\text{CH}_3\text{Hg}^+$  to the more stable  $\text{Hg}^{2+}$  form.<sup>55</sup>

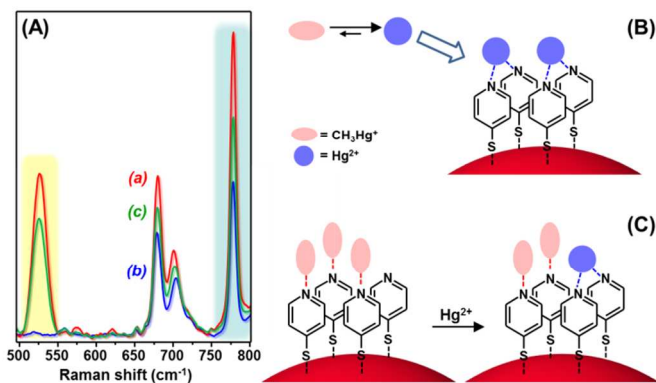


**Fig. 5** (A) SERS spectra in the 500–800  $\text{cm}^{-1}$  range of MPY on PS@Au beads upon the addition of (a)  $\text{CH}_3\text{Hg}^+$  (12 ppb, final concentration) and (b) a mixture of  $\text{Hg}^{2+}$  and  $\text{CH}_3\text{Hg}^+$  (3 ppb and 12 ppb, respectively, final concentration). (c) SERS spectrum acquired upon the addition of  $\text{Hg}^{2+}$  (3 ppb, final concentration) to the sample (a). Final concentration of beads in solution = 0.8  $\mu\text{g}/\text{mL}$ . SERS spectra are normalized to the ring breathing band at 1096  $\text{cm}^{-1}$ . (B) and (C) Schematic outlines of the coordination processes corresponding to the spectra (b) and (c), respectively.

## Experimental

**Materials.** All chemicals were purchased from Sigma-Aldrich and used as received. Milli-Q water was used throughout the experiments.

**Synthesis of Au colloids.** Small gold nanoparticles (Au seeds) of ~15 nm diameter were prepared according to the Turkevich-Frens preparation method.<sup>56, 57</sup> Briefly,  $\text{HAuCl}_4$  trihydrate (15 mg) was dissolved in milli-Q water (150 mL) and heated to boiling. An aqueous solution of trisodium citrate (1% w/w, 4.5 mL) was then quickly added under vigorous stirring, and the mixture was refluxed for 30 more minutes. The solution was then allowed to cool to room temperature under gentle stirring for several hours. Large gold nanoparticles of  $55 \pm 3$  nm (Figure S1) were prepared by following the previously reported seeded growth method.<sup>28</sup> Briefly, 125 mL of a solution of  $\text{HAuCl}_4$  trihydrate (14.57 mg) in milli-Q water were heated to boiling; then, under vigorous stirring, 3.75 mL of Au seeds and 2.56 mL of an aqueous solution of trisodium citrate (1% w/w) were consecutively added to the solution. The mixture was refluxed for 30 minutes before adding 4.3 mL of a 4.6% w/w trisodium citrate aqueous solution. The solution was finally allowed to boil for another hour and let to cool down to room temperature under gentle stirring for several hours.

**Assembly of PS@Au microbeads.** Polystyrene microbeads of 3  $\mu\text{m}$  diameter (0.5 mL of a 100 mg/mL suspension) were first wrapped with alternating polyelectrolyte monolayers using the layer-by-layer (LbL) electrostatic self-assembly protocol.<sup>37, 58</sup> Alternate layers of negatively charged polystyrenesulfonate (PSS, Mw = 1000000) and positively charged branched-polyethylenimine (PEI, Mw = 25000) were deposited in the following order: PSS, PEI, PSS and PEI. Specifically, polystyrene microbeads (0.5 mL of a 100 mg/mL suspension) were added to 25 mL of a 2 mg/mL PSS aqueous solution containing 0.5 M NaCl. After 30 min of sonication and 2 hours

of agitation, the PS microbeads were extensively washed with milli-Q water and centrifuged (5800 rpm, 20 min). Identical protocol (concentrations, elapsed times, and washing protocol) was applied for depositing subsequent layers of polyelectrolytes. Finally, the PS beads were redispersed in 10 mL of milli-Q water (final concentration 5 mg/mL).

The adsorption of the particles onto the polyelectrolytes-wrapped PS beads (5 mg/mL) was carried out by adding a large excess of Au colloids in order to achieve the highest possible surface coverage density onto the PS beads. Specifically, 10 mL of PS beads 5 mg/mL were added to 50 mL of 55 nm diameter Au NPs. After 30 min of sonication, the PS@Au beads were left under shaking for 2 hours and then left it at rest overnight for decantation. The clear supernatant was removed and the whole process was repeated four more times until the supernatant retained a reddish color characteristic of gold colloids in suspension. Then, the mixture was washed first for three times by centrifugation (2000 rpm, 25 min) and subsequently three times more by decantation with milli-Q water to remove any unbound Au NPs from the mixture. The samples were finally redispersed to 10 mL in milli-Q (5 mg/mL final concentration of PS@Au beads). Representative TEM and ESEM images of PS@Au particles are also reported in Figure S2, whereas optical extinction spectra of PS@Au and PS suspensions, as well as Au NP colloids, are illustrated in Figure S3.

**Functionalization of PS@Au beads with 4-mercaptopyridine (MPY).** 0.4 mL of PS@Au beads (5 mg/mL) were added to 5 mL of an ethanolic solution of 4-mercaptopyridine, MPY,  $10^{-2}$  M, and left under agitation for 48 hours (the sample was also repeatedly sonicated during this aging step to guarantee optimal dispersion of the beads) in order to obtain a well-packed SAM of the ligand onto the metal surface. Extensive washing of the PS@Au-MPY beads was performed to eliminate unbound MPY molecules from the solution, which consisted in 5 centrifugation/washing steps with 10 mL of ethanol and 2 centrifugation/washing steps with 10 mL of milli-Q water. Finally, PS@Au-MPY beads were redispersed in 5 mL of milli-Q water (0.4 mg/mL). PS@Au beads functionalized with thiophenol (TP) as an experimental control were prepared following the same procedure.

**SERS detection of  $\text{Hg}^{2+}$  and  $\text{CH}_3\text{Hg}^+$  with PS@Au-MPY beads.** 10  $\mu\text{L}$  of a sonicated PS@Au-MPY suspension were added to fresh aqueous solution of  $\text{HgCl}_2$  or  $\text{CH}_3\text{HgCl}$  of variable concentration (pH ~ 7) and left under shaking for 2 hours before being centrifuged to 50  $\mu\text{L}$  (final volume) and immediately investigated by SERS. Progressively lower detection limits were obtained by increasing the analyte volume solutions from 0.5 mL to 10 mL and, finally, to 50 mL. The corresponding bead concentrations in the metal solutions were 16  $\mu\text{g}/\text{mL}$ , 0.8  $\mu\text{g}/\text{mL}$  and 0.08  $\mu\text{g}/\text{mL}$ , respectively. SERS measurements were obtained using 785 nm excitation and a long working distance objective (100% laser power, 1 accumulation, 10s exposure time). The Raman background of the plastic container (Figure S7) was subtracted from each

spectrum, although some residual weak narrow bands ascribed to the plastic still appeared in some spectra.

**Instrumentation.** SERS experiments were conducted using a Renishaw InVia Reflex confocal microscope equipped with a high-resolution grating consisting of 1200 grooves/cm for NIR wavelengths, additional band-pass filter optics, and a CCD camera. UV-vis spectra were recorded using a Thermo Scientific Evolution 201 UV-visible spectrophotometer. Transmission electron microscopy (TEM) was performed with a JEOL JEM-1011 transmission electron microscope. Environmental scanning electron microscopy (ESEM) was performed with a JEOL 6400 scanning electron microscope. Quantitative cathodoluminescence was carried out using an Attolight Rosa 4634 microscope, which tightly integrates a high-speed achromatic reflective lens (N.A. 0.72) within the objective lens of a field-emission-gun-scanning-electron microscope (FEG-SEM). Cathodoluminescence was spectrally resolved with a Czerny-Turner spectrometer (Horriba-JY iHR320, 320 mm focal length, 150 grooves/mm grating) and measured with an Andor Newton EM-CCD (EM-970P-BV). Electron beam energies of 8 kV were used to excite the samples. The beam dwell time was set to 0.2 s.

## Conclusions

In summary, we report first example of a SERS-based sensor for chemical speciation of  $\text{Hg}^{2+}$  and  $\text{CH}_3\text{Hg}^+$ . 4-Mercaptopyridine was selected as an organic chemoreceptor capable of (i) strongly binding to gold nanoparticles organized on polystyrene microbeads in highly SERS active hybrid materials and (ii) coordinating both mercury species via its aromatic nitrogen, yielding corresponding MPY- $\text{Hg}^{2+}$  and MPY-( $\text{Hg}-\text{CH}_3$ )<sup>+</sup> surface complexes with different SERS spectra. The characteristic spectral changes in the chemoreceptor SERS profile upon metal coordination enabled the effective chemical speciation between the inorganic and organic-mercury forms and were also quantitatively correlated with the metal ion concentrations for their detection at trace levels.

## Acknowledgements

This work was funded by the Spanish Ministerio de Economía y Competitividad (CTQ2011-23167), the European Research Council (CrossSERS, FP7/2013 329131, PrioSERS FP7/2014 623527), Xunta de Galicia (INBIOMED-FEDER “unha maneira de facer Europa”), and Fundación Ramón Areces and National Research Foundation, Singapore (NRF-NRFF2012-04).

## Notes and references

<sup>a</sup> Departamento de Química Física e Inorgánica, Universitat Rovira i Virgili, Avda. Països Catalans 26, 43007 Tarragona, Spain.

<sup>b</sup> CTQC - Centro de Tecnología Química de Cataluña, Carrer de Marcel·lí Domingo s/n, 43007 Tarragona, Spain.

<sup>c</sup> Departamento de Química Física, Universidade de Vigo, and Centro de Investigación Biomédica (CINBIO), 36310, Vigo, Spain.

<sup>d</sup> Division of Chemistry and Biological Chemistry, School of Physical and Mathematical Sciences, Nanyang Technological University, Singapore 637371.

<sup>e</sup> ICREA, Passeig Lluís Companys 23, 08010 Barcelona, Spain.

<sup>f</sup> ICFO - Institut de Ciències Fotoniques, Mediterranean Technology Park, 08860 Castelldefels (Barcelona), Spain.

Electronic Supplementary Information (ESI) available: Representative TEM and ESEM images of AuNPs and PS@Au particles. Optical extinction spectra of AuNPs and PS@Au suspensions. SERS spectra of unmodified PS@Au suspension before and after the addition of  $\text{CH}_3\text{Hg}^+$ . SERS spectra of PS@Au-MPY upon addition of several metal solutions. Detailed SERS study of the MPY response to high concentration of  $\text{CH}_3\text{Hg}^+$ . See DOI: 10.1039/b000000x/

## References

1. K. Leopold, M. Foulkes and P. Worsfold, *Anal. Chim. Acta*, 2010, **663**, 127-138.
2. M. Kelly, W. J. Allison, A. R. Garman and C. J. Symon, *Mining and the Freshwater Environment*, Elsevier, Essex, England 1988.
3. K. W. Jackson and T. M. Mahmood, *Anal. Chem.*, 1994, **66**, R252-R279.
4. Y. Gao, Z. M. Shi, Z. Long, P. Wu, C. B. Zheng and X. D. Hou, *Microchem J.*, 2012, **103**, 1-14.
5. ATSDR (Agency for Toxic Substances and Disease Registry), Priority List of Hazardous Substances, <http://www.atsdr.cdc.gov/spl/>.
6. European Commission, Priority substances under the Water Framework Directive, [http://ec.europa.eu/environment/water/water-framework/priority\\_substances.htm](http://ec.europa.eu/environment/water/water-framework/priority_substances.htm).
7. A. J. Poulain and T. Barkay, *Science*, 2013, **339**, 1280-1281.
8. M. Leermakers, W. Baeyens, P. Quevauviller and M. Horvat, *Trac-Trends Anal. Chem.*, 2005, **24**, 383-393.
9. Z. Guo, Z.-G. Liu, X.-Z. Yao, K.-S. Zhang, X. Chen, J.-H. Liu and X.-J. Huang, *Sci Rep*, 2013, **3**, 3115.
10. J. S. Lee, M. S. Han and C. A. Mirkin, *Angew. Chem.-Int. Edit.*, 2007, **46**, 4093-4096.
11. X. J. Xue, F. Wang and X. G. Liu, *J. Am. Chem. Soc.*, 2008, **130**, 3244-3245.
12. H. N. Kim, W. X. Ren, J. S. Kim and J. Yoon, *Chem. Soc. Rev.*, 2012, **41**, 3210-3244.
13. C. Diez-Gil, R. Martinez, I. Ratera, T. Hirsh, A. Espinosa, A. Tarraga, P. Molina, O. S. Wolfbeis and J. Veciana, *Chemical Communications*, 2011, **47**, 1842-1844.
14. Y. K. Yang, K. J. Yook and J. Tae, *J. Am. Chem. Soc.*, 2005, **127**, 16760-16761.
15. L. Zhang, H. X. Chang, A. Hirata, H. K. Wu, Q. K. Xue and M. W. Chen, *ACS Nano*, 2013, **7**, 4595-4600.
16. W. Ren, C. Z. Zhu and E. K. Wang, *Nanoscale*, 2012, **4**, 5902-5909.
17. T. Senapati, D. Senapati, A. K. Singh, Z. Fan, R. Kanchanapally and P. C. Ray, *Chemical Communications*, 2011, **47**, 10326-10328.
18. D. Han, S. Y. Lim, B. J. Kim, L. Piao and T. D. Chung, *Chemical Communications*, 2010, **46**, 5587-5589.

19. E. Chung, R. Gao, J. Ko, N. Choi, D. W. Lim, E. K. Lee, S. I. Chang and J. Choo, *Lab Chip*, 2013, **13**, 260-266.
20. V. M. Zamarion, R. A. Timm, K. Araki and H. E. Toma, *Inorg. Chem.*, 2008, **47**, 2934-2936.
21. S. Botasini, G. Heijo and E. Mendez, *Anal. Chim. Acta*, 2013, **800**, 1-11.
22. K. A. Willets and R. P. Van Duyne, *Annu. Rev. Phys. Chem.*, 2007, **58**, 267-297.
23. M. Moskovits, *Rev. Mod. Phys.*, 1985, **57**, 783-826.
24. R. A. Alvarez-Puebla and L. M. Liz-Marzan, *Energy Environ. Sci.*, 2010, **3**, 1011-1017.
25. R. A. Alvarez-Puebla and L. M. Liz-Marzan, *Small*, 2010, **6**, 604-610.
26. S. Abalde-Cela, P. Aldeanueva-Potel, C. Mateo-Mateo, L. Rodriguez-Lorenzo, R. A. Alvarez-Puebla and L. M. Liz-Marzan, *J. R. Soc. Interface*, 2010, **7**, S435-S450.
27. K. Saha, S. S. Agasti, C. Kim, X. N. Li and V. M. Rotello, *Chem. Rev.*, 2012, **112**, 2739-2779.
28. Z. Krpetic, L. Guerrini, I. A. Larmour, J. Reglinski, K. Faulds and D. Graham, *Small*, 2012, **8**, 707-714.
29. D. Tsoutsi, L. Guerrini, J. M. Hermida-Ramon, V. Giannini, L. M. Liz-Marzan, A. Wei and R. A. Alvarez-Puebla, *Nanoscale*, 2013, **5**, 5841-5846.
30. D. Tsoutsi, J. M. Montenegro, F. Dommershausen, U. Koert, L. M. Liz-Marzan, W. J. Perak and R. A. Alvarez-Puebla, *ACS Nano*, 2011, **5**, 7539-7546.
31. R. A. Alvarez-Puebla and L. M. Liz-Marzan, *Angew. Chem.-Int. Edit.*, 2012, **51**, 11214-11223.
32. T. Ibusuki and Y. Saito, *Inorg. Chim. Acta*, 1976, **19**, 87-90.
33. A. J. Canty, C. L. Raston, B. W. Skelton and A. H. White, *J. Chem. Soc.-Dalton Trans.*, 1982, 15-18.
34. D. J. Brown, *The Chemistry of Heterocyclic Compounds, Pyridine Metal Complexes*, Wiley-Interscience 1985.
35. D. L. Rabenstein, *Accounts Chem. Res.*, 1978, **11**, 100-107.
36. M. Spuch-Calvar, L. Rodriguez-Lorenzo, M. P. Morales, R. A. Alvarez-Puebla and L. M. Liz-Marzan, *J. Phys. Chem. C*, 2009, **113**, 3373-3377.
37. R. Ahijado-Guzman, P. Gomez-Puertas, R. A. Alvarez-Puebla, G. Rivas and L. M. Liz-Marzan, *ACS Nano*, 2012, **6**, 7514-7520.
38. S. Abalde-Cela, J. M. Hermida-Ramon, P. Contreras-Carballada, L. De Cola, A. Guerrero-Martinez, R. A. Alvarez-Puebla and L. M. Liz-Marzan, *ChemPhysChem*, 2011, **12**, 1529-1535.
39. H. Z. Yu, N. Xia and Z. F. Liu, *Anal. Chem.*, 1999, **71**, 1354-1358.
40. J. Kucera and A. Gross, *Langmuir*, 2008, **24**, 13985-13992.
41. J. Hu, B. Zhao, W. Xu, B. Li and Y. Fan, *Spectrochimica Acta Part A: Molecular and Biomolecular Spectroscopy*, 2002, **58**, 2827-2834.
42. Y. W. Chao, Q. Zhou, Y. Li, Y. R. Yan, Y. Wu and J. W. Zheng, *J. Phys. Chem. C*, 2007, **111**, 16990-16995.
43. J. A. Baldwin, B. Vlckova, M. P. Andrews and I. S. Butler, *Langmuir*, 1997, **13**, 3744-3751.
44. H. Guo, L. Ding and Y. J. Mo, *J. Mol. Struct.*, 2011, **991**, 103-107.
45. S. Akyuz, A. B. Dempster and S. Suzuki, *J. Mol. Struct.*, 1973, **17**, 105-125.
46. A. G. Brolo, M. Odziemkowski and D. E. Irish, *J. Raman Spectrosc.*, 1998, **29**, 713-719.
47. G. Mizutani and S. Ushioda, *The Journal of Chemical Physics*, 1989, **91**, 598-602.
48. M. Moskovits, *J. Chem. Phys.*, 1982, **77**, 4408-4416.
49. M. Moskovits and J. S. Suh, *J. Phys. Chem.*, 1984, **88**, 5526-5530.
50. A. J. Canty and A. Marker, *Inorg. Chem.*, 1976, **15**, 425-430.
51. A. J. Canty and C. V. Lee, *Organometallics*, 1982, **1**, 1063-1066.
52. J. Bjerrum, *Acta Chem. Scand.*, 1972, **26**, 2734-2742.
53. S. Alex and R. Savoie, *Can. J. Chem.-Rev. Can. Chim.*, 1987, **65**, 491-496.
54. U. S. E. P. A. (EPA), 2009.
55. W. Stumm and J. J. Morgan, *Aquatic Chemistry: Chemical Equilibria and Rates in Natural Waters*, John Wiley & Sons 1995.
56. J. Turkevich, P. C. Stevenson and J. Hillier, *Discussions of the Faraday Society*, 1951, 55-75.
57. G. Frens, *Nature-Physical Science*, 1973, **241**, 20-22.
58. G. Decher, *Science*, 1997, **277**, 1232-1237.